NASA-CR-194253

GaAs/AlGaAs Heterostructure Point Contact Concentrator Cells

NASA Contract NAS3-25449
SBIR-10.02-6696
Release Date 8/20/92

Final Report

SBIR 1986 Phase II

KOPIN CORPORATION
695 Myles Standish Boulevard
Taunton, Massachusetts 02780

by:

Ronald Gale and Mark Spitzer

Prepared for:
NASA-Lewis Research Center
Cleveland, Ohio 44135

ABSTRACT

GaAs is a strong contender for use in space photovoltaic power systems due to its high conversion efficiencies, radiation hardness, and developed processing technology. This document reports on the research of high-efficiency thin-film GaAs concentrator cells for space applications. Thin-film AlGaAs-GaAs double-heterostructure concentrator cells were fabricated which exhibit total-area conversion efficiencies as high as 23.5% AM0 at 100 suns, 25°C, measured at NASA. This solar cell structure consists of a GaAs/AlGaAs film less than 5um thick mounted to a glass cover/superstrate, with coplanar back-side contacts. The coverglass is not prismatic. We use the CLEFT process, a method for mechanically separating epitaxial layers from their substrate, to process these cells into thin-films. We thereby retain the advantages of single-crystal GaAs while reducing weight and cutting cost by allowing for substrate reuse. Thin film cells also have better thermal management capabilities and can be stacked for use in tandem structures. Research on material and junction formation is described, as are the resulting cell fabrication and performance.

ACKNOWLEDGEMENTS

The authors would like to thank L. Allen, M. Boden, D. Brandt, B. Dingle, J. Dingle, J. Fan, A. Foley, S. Foster, J. Gormley, M. Knowles, J. Mannino, R. McClelland, K. McDavitt, R. Morrison, T. Nunes, K. O'Connor, J. Salerno, J. Westcoat, and M. Zavracky, all of Kopin, for their contributions to this work. The administrative support of C. Davis and C. Brothers is gratefully acknowledged. In addition, the authors acknowledge the support and guidance of H. Curtis of the NASA Lewis Research Center.

TABLE OF CONTENTS

LIST OF FIGURES

LIST OF TABLES

SECTION 1: Introduction

We have routinely used the CLEFT [1-3] process to produce thin film semiconductor materials up to three inches in diameter and less than 10 μm thick. CLEFT is an established process which entails the mechanical separation of the epitaxial film from its substrate. This approach has the benefit of allowing for substrate reuse, thereby reducing the overall cell material cost. We have now applied the CLEFT process to the fabrication of concentrator cells in order to take advantage of the inherent benefits of thin-film cells. By "thin-film" we mean layers less than 10 um thick that are removed entirely from a single crystal substrate. Thin-film concentrator cells are of interest because they require less than 5 μm of semiconducting material and their efficiencies are now comparable to cells on bulk substrates.

The extremely thin nature of these cells also allows for low weight and superior thermal management. Heat sinking can be more effective because it can be placed in closer proximity to the junction. Since the cells are transparent to long wavelenths, infra-red radiation which enters the cell can be transmitted directly to a back-side heat sink or, alternatively, reflected out the front of the cell by using a back surface reflector. A back surface reflector could also be tailored to reflect photons with energy above the band edge, thus providing a double pass for more weakly absorbed light, thereby doubling the effective material thickness. Ultimately, thin film cells can be expected to yield higher efficiencies than conventional cells owing to light trapping possibilities or lower operating temperature. These thin-film cells also lend themselves well to tandem structures and advanced structures involving reflectors and coplanar contacts.

This document is the final report for NASA Small Business Innovative Research contract # NAS3-25449 to develop thin-film photovoltaic concentrator cells designs based on a point-contact approach. The goal of this contract was to demonstrate a high-efficiency thin-film space concentrator cell. The specific objectives of this contract were the development of materials and device technology necessary to make possible such a cell, particularly using the point-contact approach. The technology developed here includes:

- o research on high-diffusion length GaAs,
- o investigation of patterned junction formation,
- o development of co-planar p and n contact formation based on utilizing the CLEFT process for thickness reduction, and
- o fabrication of prototype photovoltaic cells.

The project was organized in five tasks, which are indicated in Table 1. The objectives of these tasks have been achieved, and the project has resulted in the fabrication of high-efficiency thin-film concentrator cells. This report has integrated these tasks into four main sections, including Materials Research, Junction Formation, Inverted Cell, and Thin-Film Concentrator Cell. Modelling, metallization, and cell fabrication are included as appropriate in the two sections on cells. CLEFT processing is first described below in Section 2. Publications resulting from this work are provided in the appendix.

TABLE 1
PROGRAM TASKS AND OBJECTIVES

TASK	OBJECTIVES
1. Research on Materials	Obtain high-lifetime GaAs and low recombination velocity at AlGaAs-GaAs interfaces, on CLEFT wafers.
2. Junction Formation	Develop patterned junction fabricated techniques for point-contact formation.
3. Modelling and Characterization	Obtain understanding of material properties and optimized structure.
4. Metallization	Develop compatible metallization and design masks.
5. Cell Fabrication	Integrate processes and fabricate test cells.

SECTION 2: Cleft Processing

The Cleavage of Laterally-overgrown Films for Transfer (CLEFT) process permits the separation of a thin single-crystal film, grown by chemical vapor deposition (CVD), from a reusable homoepitaxial substrate. In the CLEFT process, the substrate wafer is recovered and reused; therefore many thin-film cells can be obtained from one substrate. For this reason, the CLEFT technique makes possible a large reduction in material usage and cost. In fact, the yield is so high with the CLEFT process that the wafer cost is not a consequential factor in the ultimate cost to fabricate the cell.

The CLEFT process, illustrated in Fig. 1 below, involves the following steps: growth of the desired thin film over a release layer (a plane of weakness), formation of metallization and antireflection (AR) coating, formation of a bond between the film and a coverglass (or superstrate), and separation along the built-in plane of weakness by cleaving. The substrate is then available for reuse.

The key element that makes the CLEFT process possible is the use of lateral epitaxial growth to form a continuous single-crystal film on top of a release layer. This process requires a mask to limit film nucleation to a small fraction of the wafer surface. Our experiments on GaAs have shown that if a mask with appropriately spaced stripe openings is deposited on a properly oriented GaAs substrate, the epitaxial growth initiated on the GaAs surface exposed through the openings will be followed by lateral growth over the mask, and will eventually produce a continuous single-crystal film that can be grown to any desired thickness. The overgrowth of an epitaxial film is illustrated in Fig. 2. Under the growth conditions used for present-day GaAs, the ratio of lateral to vertical growth rates is about 10 to 1, so that the film becomes

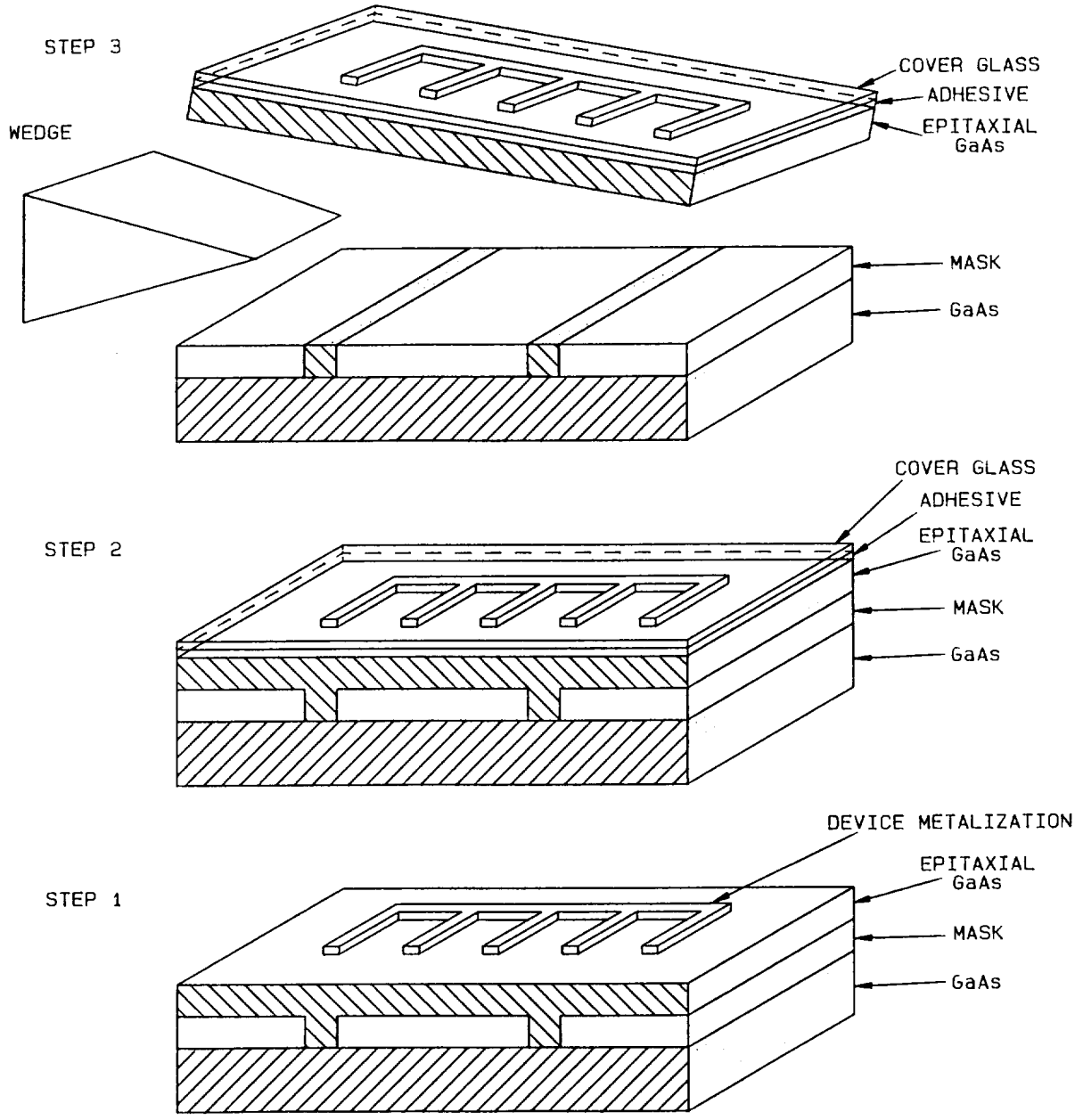

FIGURE 1. **ILLUSTRATION OF THE CLEFT PROCESS.** First, the desired film is laterally grown over a built-in plane of weakness. Second, processing such as metallization or AR coating is carried out. Third, the wafer is bonded to a coverglass. Finally, the film and the substrate are separated by cleaving. The substrate can be reused.

continuous when it is only about 3 microns thick.

One of the necessary properties of the foreign film that forms the mask is the lack of adhesion between the mask material and the film. In such a case, the film will be strongly attached to the substrate only at the stripe openings. Since a weak plane has been created by the mask, the film can be cleaved from the substrate without any degradation.

After epitaxial growth of the required p-n junction and other layers, the structure is partially fabricated into a device. Metallization and AR coatings are applied to the front surface. The upper surface of the film is bonded with a transparent epoxy to a superstrate such as glass. The film and glass are then bonded with wax to glass plates about 5 mm thick that serve as cleaving supports. A metal wedge is inserted between the two glass plates to force the surfaces apart. Since the mask has low adhesion to the substrate, the film is cleaved from the substrate but remains mounted on the glass. The substrate can then be used for another cycle of the CLEFT process, and the cell processing is completed on the back surface of the film. Note that since the partially completed cell remains attached to a superstrate, the back side can be subjected to standard wafer processing, including photolithography.

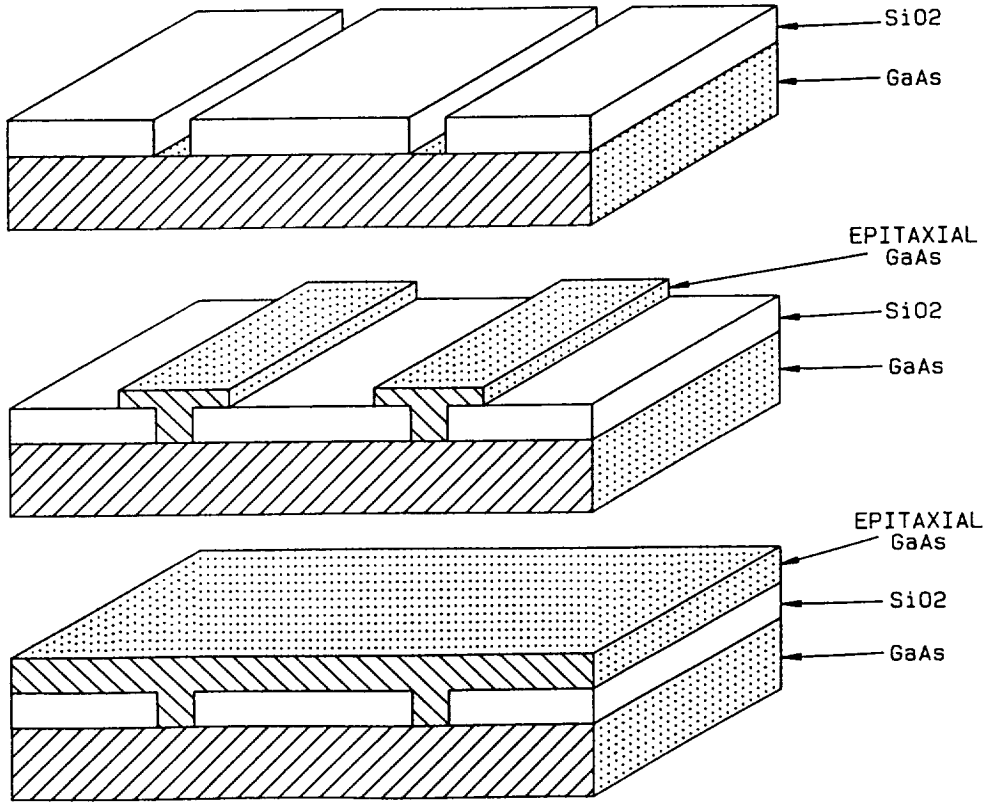

FIGURE 2. ILLUSTRATION OF THE LATERAL EPITAXIAL OVERGROWTH PROCESS. The wafer is first provided with a release layer mask. The epitaxial film is grown in the seed openings under conditions which prevent nucleation on the mask. The film continues to grow and upon reaching the top of the mask, grows laterally across the surface, until the film becomes continuous and smooth.

SECTION 3: Materials Research

A key building block of this work was the research on thin-film material quality. Device requirements in a thin-film co-planar approach include long minority-carrier lifetimes and low interface-recombination velocities. In order to characterize our layers, both room-temperature photoluminescence (PL) and photoluminescence decay techniques were used. The latter measurements were carried out at the Solar Energy Research Institute under the direction of Dr. R. Ahrankiel. A description of this technique can be found in reference 4.

Sample Preparation

Samples were grown by OMCVD on CLEFT release substrates. The structure consisted of a double heterostructure which was formed by growing first a p-doped AlGaAs passivating layer, followed by a p-doped GaAs layer (the active layer to b e tested), and capped by a second p-doped passivating AlGaAs layer. The layer to be tested was therefore confined between AlGaAs wide-bandgap barriers, which reduced interface recombination effects.

For the first set of samples, the active layers were doped at levels between $1X10^{17}$ and $6X10^{17}$ cm^{-3}, and two thicknesses of 2 and 4 um were grown. These thicknesses were chosen as they cover the range of the anticipated cell base thickness, and also allowed the lifetime of the active layer and the average interface recombination velocity to be calculated. Prior to the PL decay measurement, the samples were characterized by room-temperature PL. PL signals were high on all samples tested, indicating that the electronic quality of the baseline material was good and that the interface recombination was low. Uniformity of the PL signal across the sample was also very satisfactory.

PL Results

Results of the PL decay measurements for the first set of samples are tabulated in Table 2 below. By measuring lifetimes on two samples of different thicknesses with the same doping, the contributions of the bulk recombination and surface recombination have be calculated. As expected, the calculated bulk lifetimes increase with decreasing doping. The calculated recombination velocities at the GaAs/AlGaAs interfaces also show a strong dependence on base doping, with a very low velocity for the lowest doped sample. These results indicated that additional experiments on lower doped samples were desirable.

Additional CLEFT thin-film samples were therefore prepared for minority-carrier lifetime measurements. These included layers doped with zinc to levels of $2x10^{16}$ and $4x10^{17}$ cm^{-3}. The layers were separated from their substrates and measured using the photoluminescence decay technique. Again, layers with thicknesses of 2 and 4 um were measured in order to model bulk lifetimes and interface recombination velocities.

The lifetime data for this set of samples varied significantly, with calculated bulk lifetimes from 20 to 310 ns. Recombination velocities were higher than expected at 3000 to 11500 cm/s. The cause of these differences was attributed to variations in surface morphology and defect densities in the layers. Measurements on control samples with smooth surfaces and $2x10^{16}$ cm^{-3}

TABLE 2
RESULTS OF PHOTOLUMINESCENCE MEASUREMENTS

MEASUREMENTS			MODEL RESULTS	
Doping (cm^{-3})	Thickness (um)	PL Lifetime (nsec)	Bulk Lifetime (nsec)	Interface Recomb. Velocity (cm/sec)
$1.1X10^{17}$	2	63.5	81	342
$1.1X10^{17}$	4	71.3		
$1.8X10^{17}$	2	34.8	67	1380
$1.8X10^{17}$	4	45.8		
$5.8X10^{17}$	2	10.0	17	4250
$5.8X10^{17}$	4	12.7		

doping produced bulk lifetimes of 140-190 ns and recombination velocities of 160-330 cm/s, better than our earlier results for slightly higher doped material in Table 2. These results indicate that the lower doping will produce longer lifetimes and better electrical interfaces, provided that defects which shorten the lifetime and raise the interface recombination velocity are minimized.

Variations in the surface and defect morphology appear in the overgrowth step, but can be caused by either nonoptimum growth conditions or incomplete etching of the seed lines prior to overgrowth. Both of these conditions arise from equipment limitations, and have been placed under better control with preventative maintenance programs on the respective pieces of equipment.

With controls in place, excellent material quality has been consistently obtained with CLEFT GaAs films. Material was used for the fabrication of CLEFT cells, described in later sections.

SECTION 4: Junction Formation

Two types of junction formation techniques were investigated: ion implantation and epitaxy. Both n and p-type ions were implanted to form junctions in epitaxial layers of GaAs, while n-on-p structures were grown by OMCVD for epitaxially formed junctions. The latter was one component of our baseline process, and proved to produce better junctions than were achieved by ion implantation techniques.

Ion Implantation

Ion implantation of silicon and tellurium were investigated. P-type GaAs epitaxial structures with AlGaAs back-surface field layers were grown using OMCVD and implanted with doses of 10^{14} or 10^{15} cm^{-3}. The solar cell fabrication process used a proprietary high temperature design that permitted us to anneal the ion-implanted junctions in the form of completed cells. The most important parameters for the purposes of the current approach are the V_{oc} and the series resistance. J_{sc} is not a key factor at this point because absorption in the implanted sheet will be minimized in the final cell design. The best results of this experiment are shown in Table 3 below.

TABLE 3
RESULTS OF N-TYPE ION IMPLANTATION MATRIX

Ion	Dose (cm^{-3})	Anneal (°C, min)	V_{oc} (mV)	J_{sc} (mA/cm^2)	FF (%)	Eff. (%)
Si	10^{14}	750, 10	844	22.8	66.4	9.3
Si	10^{15}	700, 20	854	20.0	74.2	9.3
Te	10^{14}	700, 5	263	0.8	44.0	0.1

Note: Insolation was AM0, 137.2 mW/cm^2, 27°C.

The silicon-implanted samples fared far better than the tellurium-implanted samples. The open-circuit voltages for the former samples were not as high as was obtained with epitaxial junctions. This may be a result of the lack of front-surface passivation as there is no AlGaAs on the surface. The dark current-voltage (I-V) characteristics of the cells were measured to determine the diode quality factor and series resistance. The I-V of the Si-implanted cell of line two in Table 3 is shown in Figure 3. The junction diode quality factor of this cell was 1.9, increasing to 4.9 at higher values of current density.

Zinc and beryllium were used for the ion implantation of n-type layers for the formation of p-on-n junctions. Again, the solar cell fabrication process used a proprietary high temperature design that permitted us to anneal the ion-implanted junctions in the form of completed cells. The best results of this experiment are shown in Table 4.

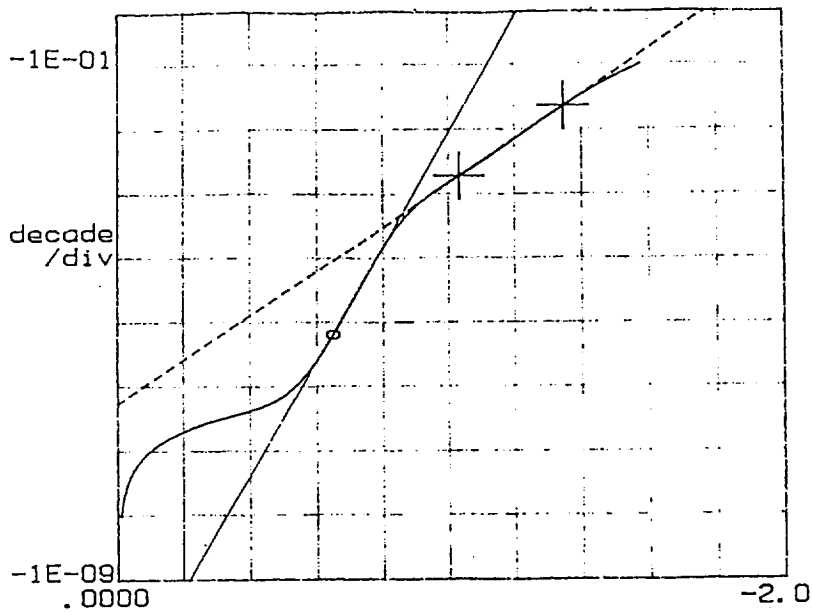

FIGURE 3. DARK I-V CHARACTERISTIC of a Si-implanted solar cell. The diode quality factor (n) is 1.9 between 0.6 and 0.8V, and 4.9 between 0.9 and 1.4V.

TABLE 4
RESULTS OF P-TYPE ION IMPLANTATION MATRIX

Ion	Dose (cm^{-3})	Anneal (°C, min)	V_{oc} (mV)	J_{sc} (mA/cm^2)	FF (%)	Eff. (%)
Zn	10^{14}	750, 5	602	2.5	51.8	0.6
Be	10^{15}	700, 1	856	18.2	79.4	9.1

Note: Insolation was AM0, 137.2 mW/cm^2, 27°C.

The dark I-V curves for these two cells are shown in Figures 4 and 5. The Be-implanted cell showed results similar to the best Si-implanted cell, but exhibited a diode quality factor of 1.3, comparable to that of junctions grown epitaxially. The diode quality factor of the Zn implant was 2.3.

Junctions grown directly by epitaxy have demonstrated the best ideality factors and have produced the highest cell voltages and efficiencies of all the junction-formation techniques investigated. For the goal of high-efficiency concentrator cells, it was clear that epitaxial junctions need to be used to meet this goal. In order to test the epitaxial junction in a configuration similar to the point-contact design, we have designed and fabricated an inverted cell structure. This structure is described in Section 5 of this report.

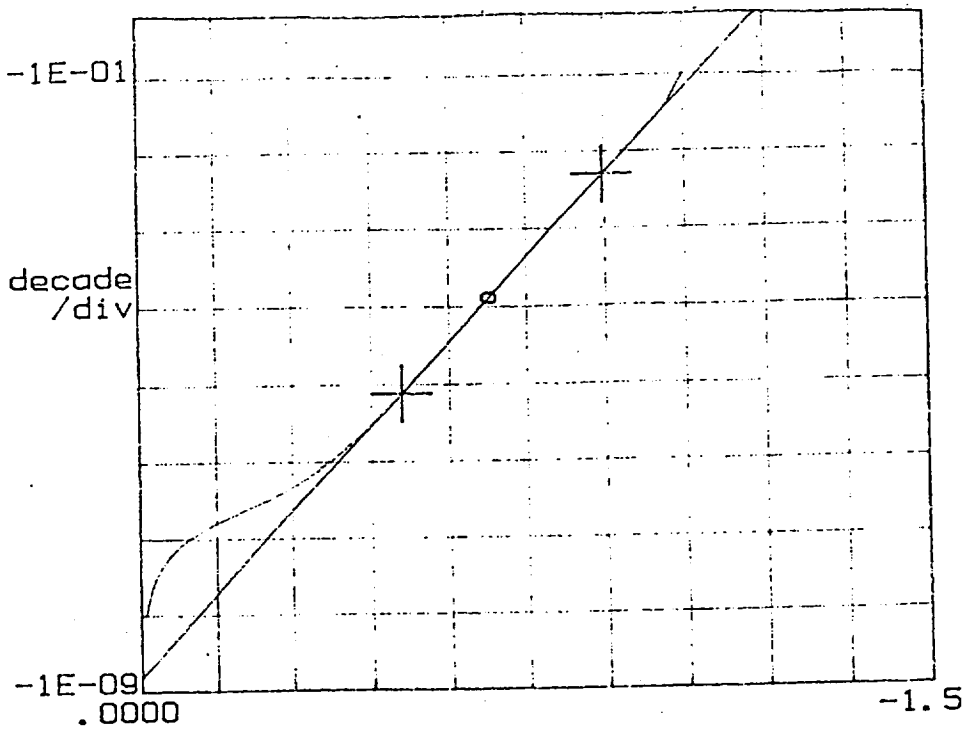

FIGURE 4. DARK I-V CHARACTERISTIC of a Zn-implanted solar cell. The diode quality factor (n) is 2.3.

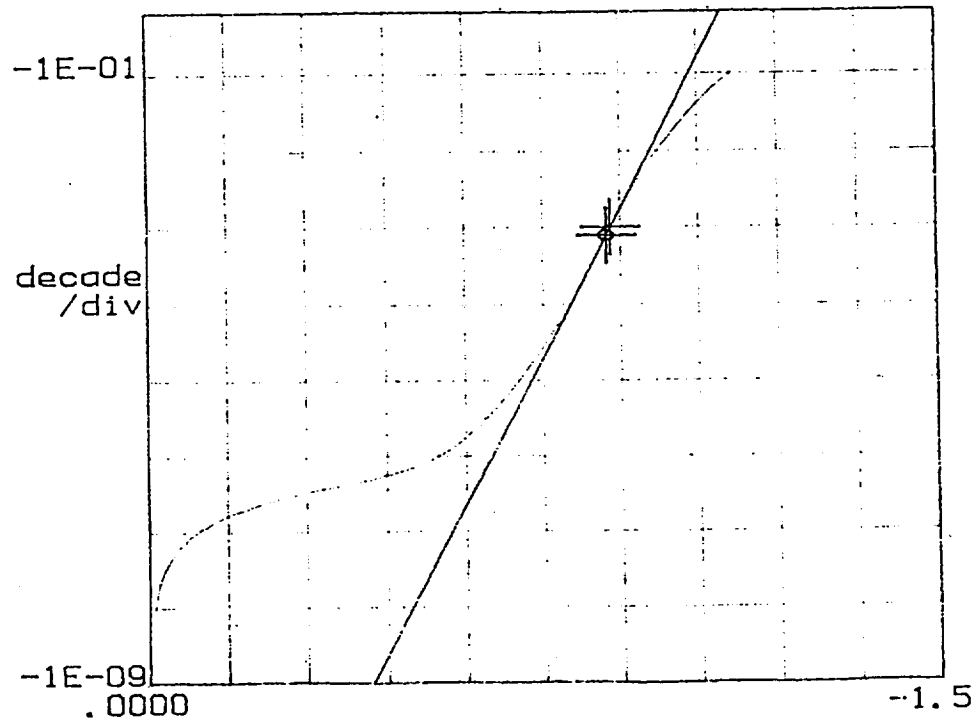

FIGURE 5. DARK I-V CHARACTERISTIC of a Be-implanted solar cell. The diode quality factor (n) is 1.3.

Baseline Cell Processing

Our baseline process used epitaxially formed junctions, as the entire solar cell structure was deposited in one OMCVD system. The baseline mask set was used to fabricate CLEFT concentrators having a diameter of 4mm (area of $0.126cm^2$). The fabrication process for these cells is shown in Table 5. Cells with both full-area and gridded back metallization were fabricated. Contact to both front and back metallization was made from the back after areas of the GaAs layer were etched away to expose the front pad.

TABLE 5
BASELINE CLEFT CELL PROCESS

1.	Lateral epitaxial overgrowth and cell layer growth.
2.	Formation of the front side collection grid.
3.	Mesa etch on the front to isolate the junction area.
4.	Deposition of the front AR coating.
5.	Coverglass addition and layer separation.
6.	Formation of the back side collection grid.
7.	GaAs removal to define the cell area and expose the front-metal bond pad.

The cells were tested under simulated AMO insolation ($137.2\ mW/cm^2$). Since these cells are covered by glass which is larger than the light-receiving area care was taken to mask the incident light so as to expose only the primary cell area. It was found that if the glass is fully exposed to the light, the incident intensity would be artificially high, owing to light collection by the glass via total internal reflection. Also, in the case of the gridded-back cell, unless the light is masked a significant amount of scattered light can enter the cell back surface and increase the current.

Figure 6 shows the I-V characteristic of a CLEFT concentrator under 18.5 suns AMO illumination. This cell has an ordinary grid on the front, and a full-area Au-metal contact on the back. The efficiency is 17.8% at one sun and 18./8% at 18.5 suns. Figure 7 shows the results of a first attempt to fabricate a transparent CLEFT concentrator cell with grids on both sides. Although the J_{sc} is limited, perhaps because the cell is too thin, the fabrication experiment shows that the CLEFT process is suitable for two-sided processing of the type needed for advanced structures. These efficiencies obtained at this point were a strong indicator of the potential of this approach.

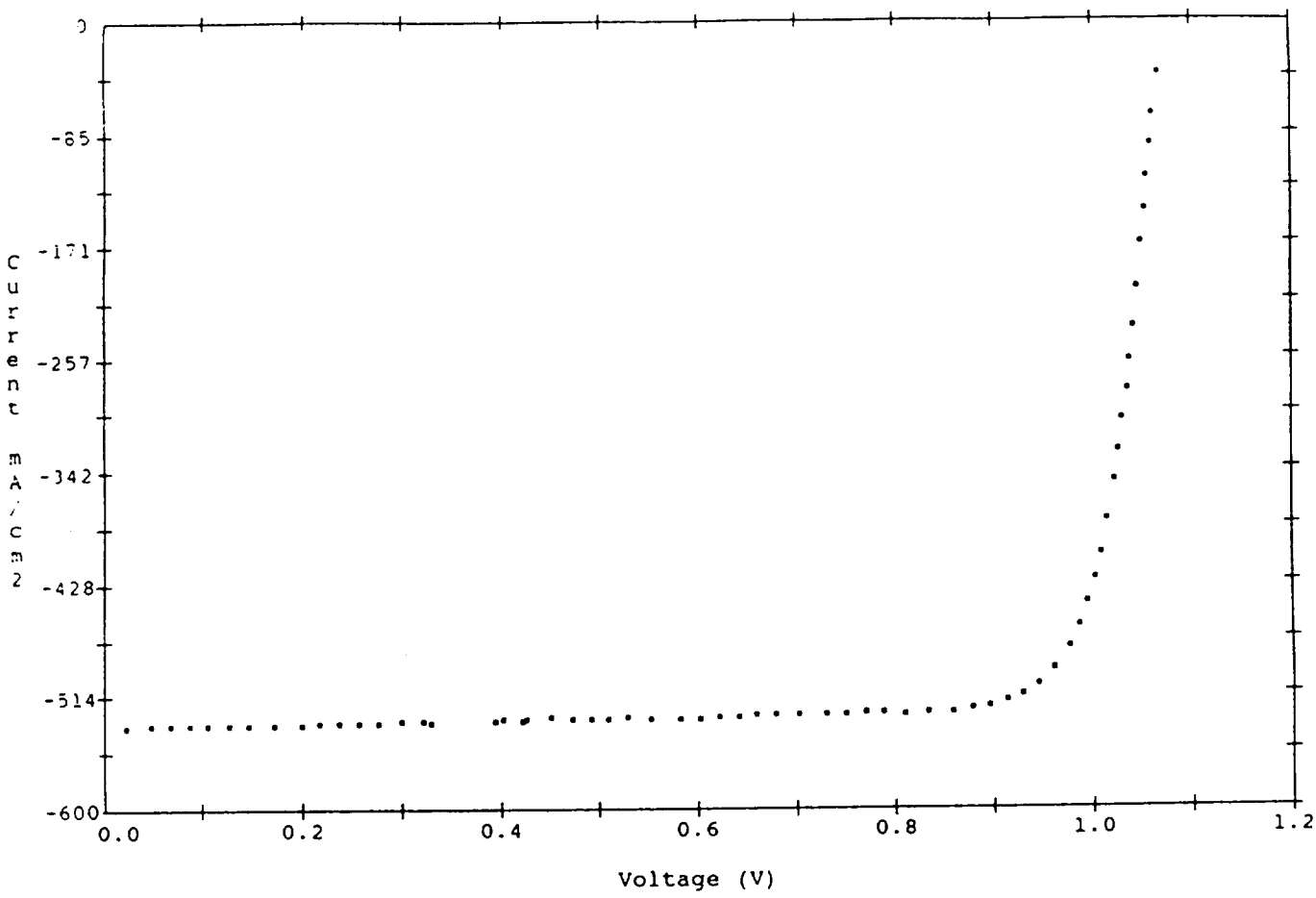

FIGURE 6. ILLUMINATED I-V CHARACTERISTIC OF A CLEFT CONCENTRATOR with baseline processing and an epitaxially formed junction. The back metal is full area. The efficiency is 18.8%, FF is 85.3%, V_{oc} is 1.044V, J_{sc} is 0.536A/cm^2, and the area of the cell is 0.126cm^2 (18.5 suns AM0, 137.2 mW/cm^2, 28°C).

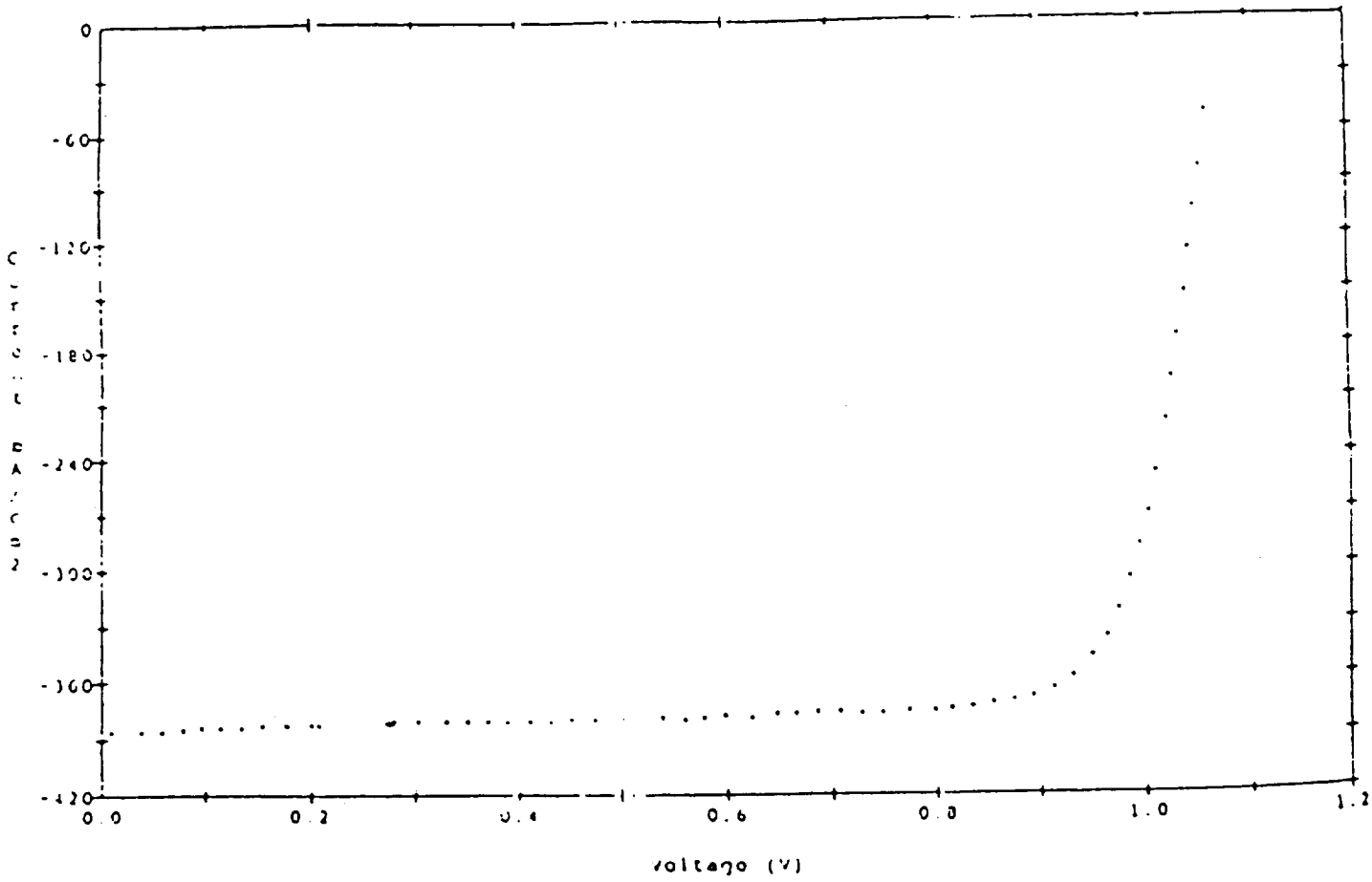

FIGURE 7. ILLUMINATED I-V CHARACTERISTIC OF A GRIDDED-BACK CLEFT CONCENTRATOR with baseline processing and an epitaxially formed junction. The efficiency is 17.1%, FF is 83.6%, V_{oc} is 1.034V, J_{sc} is 0.384A/cm^2, and the area of the cell is 0.126cm^2 (14.2 suns AM0, 137.2 mW/cm^2, 28°C).

SECTION 5: Inverted Cell Structure

In order to test the epitaxial junction in a configuration similar to the point-contact design, we designed and fabricated an inverted-junction cell (or inverted-cell) structure. In this structure, the junction is below the cell base and about four microns from the cell front surface. A schematic of the epitaxial structure grown on an N-doped substrate is shown in Figure 8. This cell structure was modeled and fabricated, as described below.

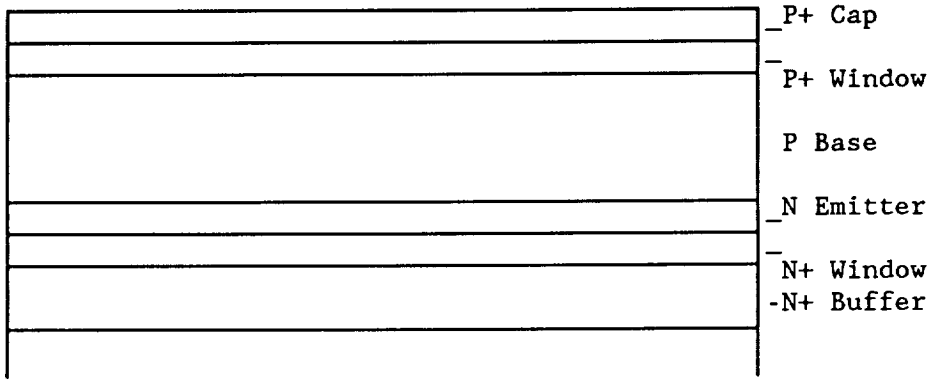

Figure 8. EPITAXIAL STRUCTURE OF THE INVERTED-JUNCTION CELL.

Inverted Cell Modeling

The inverted-junction structure was modeled under one-sun illumination for the range of base thicknesses from 0.2 to 7.0 um. Predicted one-sun cell efficiencies ranged from 15.1 to 20.5% with the short-circuit current being the determining parameter; the voltage and fill factor were largely independent of the base thickness. Figure 9 shows the predicted short-circuit current as a function of base thickness for the structures modeled. There is a broad peak in current around 31.5 mA/cm^2 for base widths between 2 and 6 um. The falloff at small thicknesses is due to loss of long-wavelength photons which are not absorbed; this is clearly shown by the internal quantum efficiencies for these structures, shown in Figure 10. For the large base thicknesses, the loss of current is across all photon wavelengths, indicating that charge collection is diffusion-length limited in the base. The minority-carrier diffusion length used for these calculations is 30 um, still in excess of the largest modeled base width of 7 um.

The importance of the base region is confirmed by analysis of where the current is generated. The predicted short-circuit current was separated into three components, generated in the base, space-charge region, and emitter. Figure 11 shows these three currents normalized to the total current, as a function of base width. Above 2 um of base thickness, over 99% of the cell current is generated in the base.

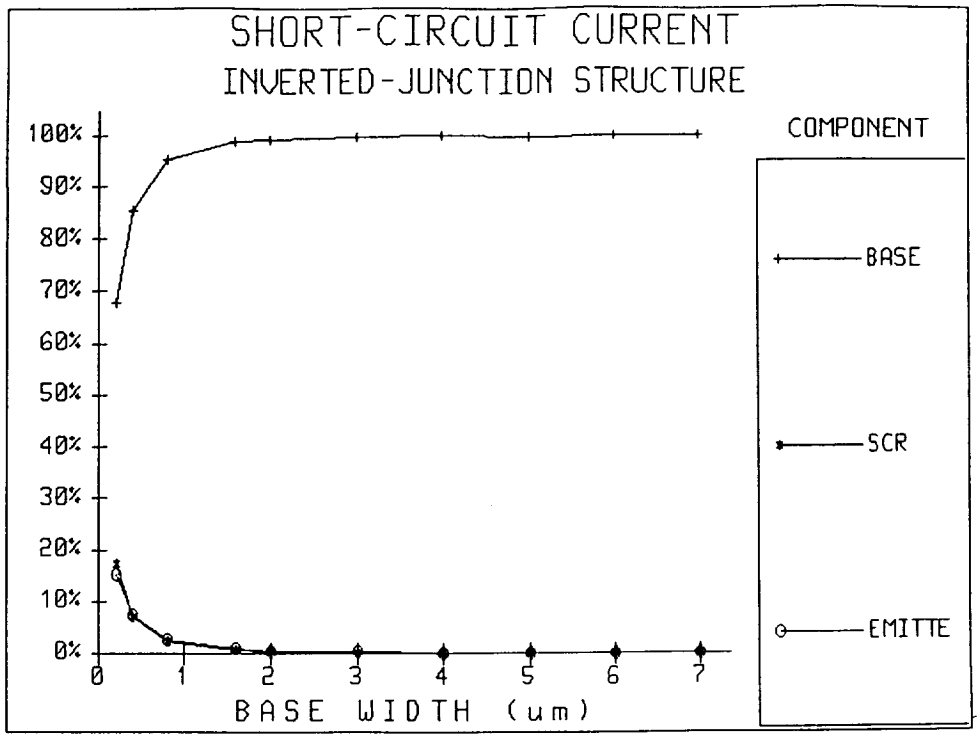

Figure 9. PREDICTED SHORT-CIRCUIT CURRENT as a function of base thickness for the modeled inverted-junction structures.

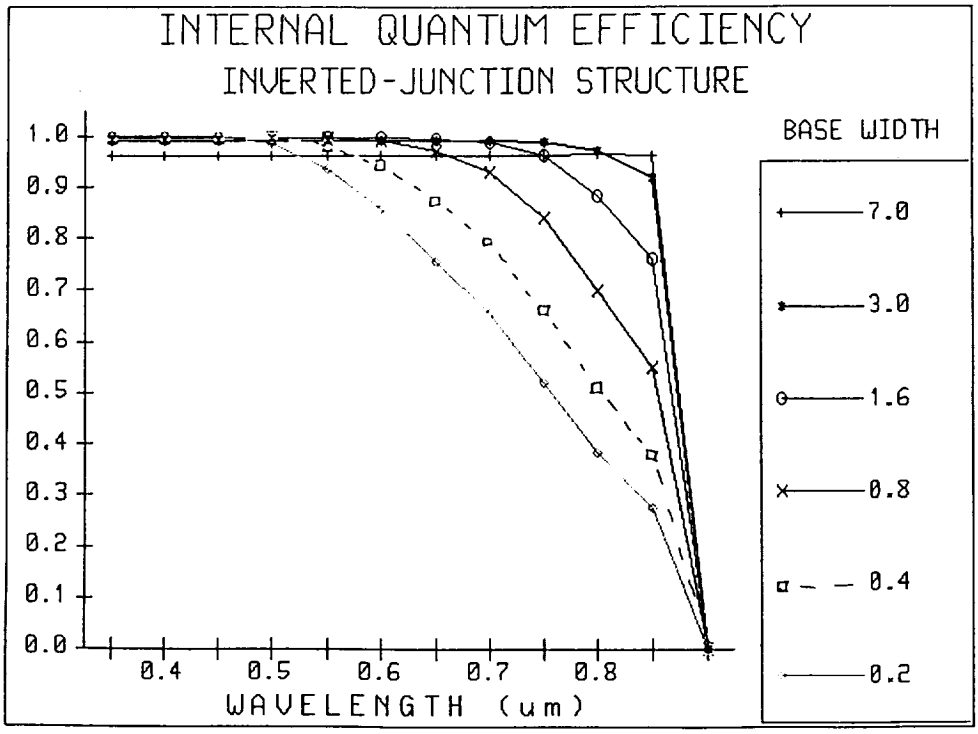

Figure 10. PREDICTED INTERNAL QUANTUM EFFICIENCIES for different base thicknesses for the modeled inverted-junction structures.

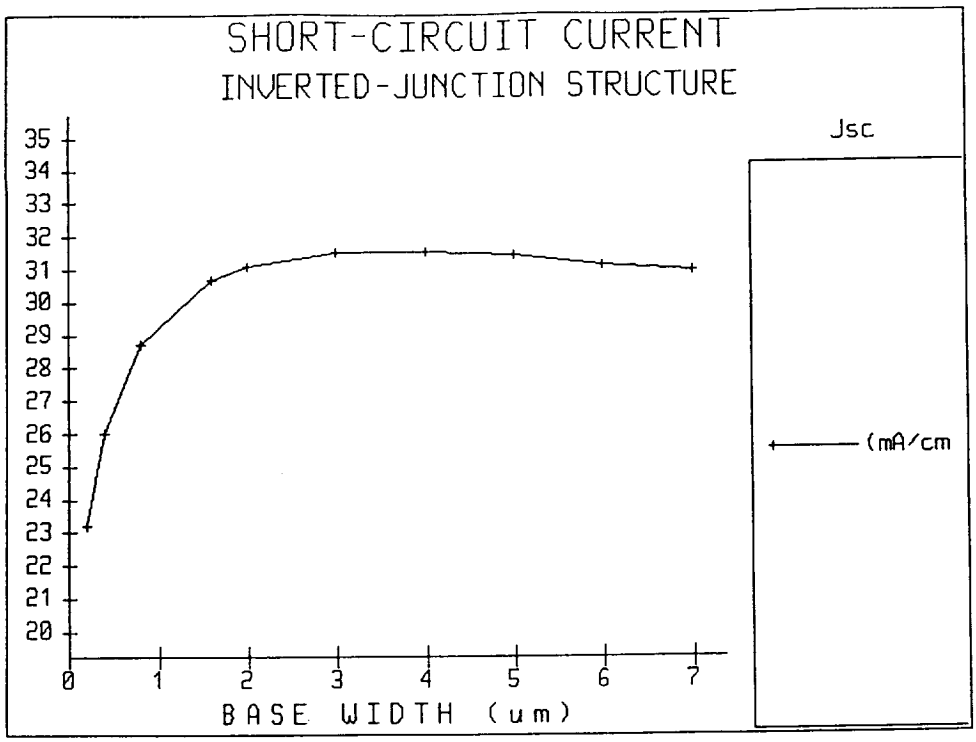

Figure 11. PREDICTED SHORT-CIRCUIT CURRENT CONTRIBUTIONS from the base, space-charge region, and emitter, as a function of base width. The currents are normalized to the total current. as a function of base width.

Inverted-Cell Fabrication

The baseline mask set was used to fabricate concentrators from the inverted-junction epitaxial structure. The fabrication process for these cells is shown in Table 6. The base width for these cells was 3 um. Cells with area of 0.126 cm^2 and complete back metallization were fabricated. A single nitride AR coating was used, with no coverglass on the cell.

TABLE 6
INVERTED-JUNCTION CELL PROCESS

1.	Inverted-junction cell layer growth
2.	Plating of the front-side collection grid
3.	Cell definition by mesa etching
4.	Plating of the front-side
5.	Deposition of front AR coating

The cells were tested under simulated AM0 insolation (137.2 mW/cm^2). The cells ranged in one-sun efficiency from 17.2 to 17.8%, and peaked in efficiency at 18.8% at 5 to 6 suns. Figure 12 shows the I-V characteristic of an inverted-junction concentrator under one-sun illumination. The cell had an efficiency of 17.8%, with a V_{oc} of 0.981 V, a J_{sc} of 29.5 mA/cm^2, and a fill factor of 84.1%. This efficiency is limited primarily by the current, which our model predicted to be 31.5 mA/cm^2 for the cell base thickness of 3 um. The external quantum efficiency of a cell from this lot is shown in Figure 13. Although this performance is quite good considering that the junction depth for this cell is 3 um, the falloff in the short-wavelength section of the spectrum indicates that more work is needed to improve this particular cell structure. The falloff could be due to either (1) a non-optimum AR coating, (2) a P-window/P-base interface recombination velocity larger than the 1E10^4 cm/sec used in the model, or (3) a non-optimum P+ window. The overall level of the quantum efficiency suggests that the P+ window is absorbing some of the incoming spectrum.

Figure 14 shows the illuminated I-V curve of the cell of Figure 12 under about 6 suns AM0. The cell had an efficiency of 18.8%, with a V_{oc} of 1.040 V, a J_{sc} of 172.4 mA/cm^2, and a fill factor of 84.1%. The voltage increased as expected, and the fill factor remained the same for this concentration. At higher concentration levels, the fill factor began to decrease due to series resistance.

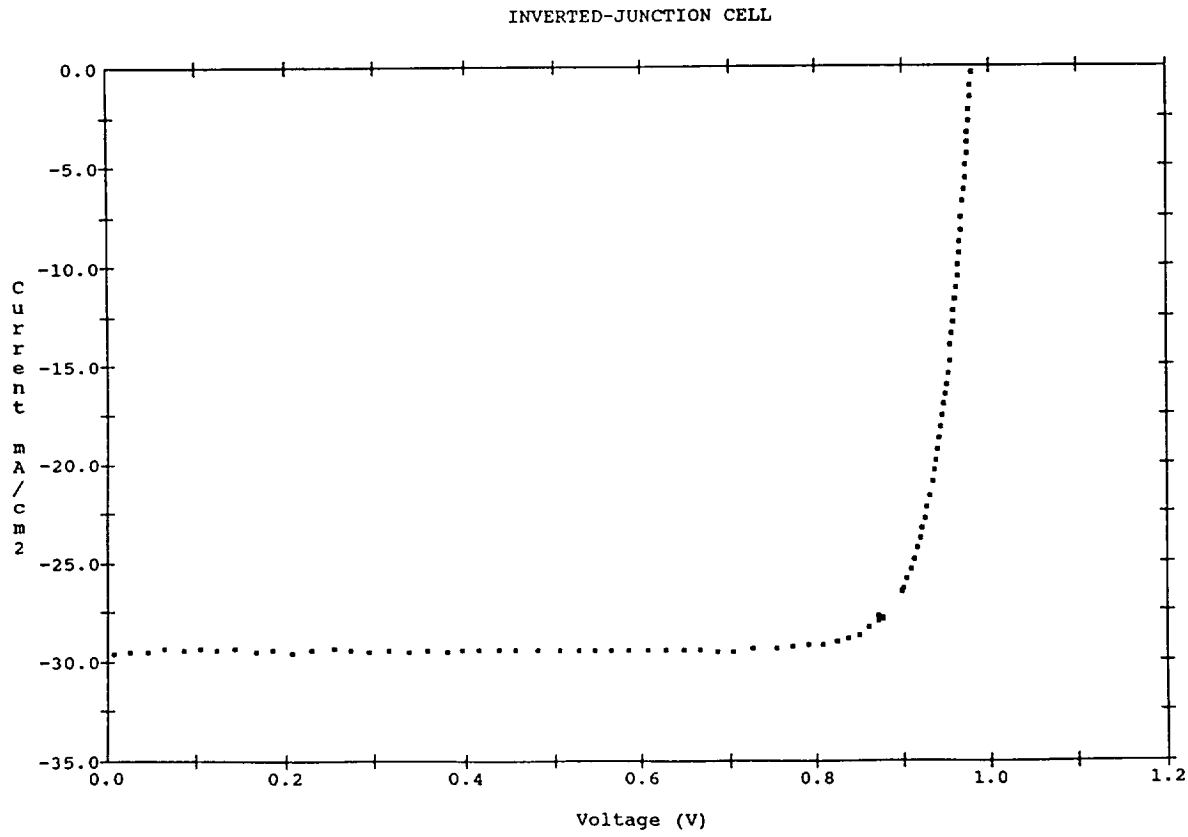

Figure 12. I-V CHARACTERISTIC OF AN INVERTED-JUNCTION CONCENTRATOR under one-sun illumination (AM0, 137.2 mW/cm^2, 28°C). The cell had an efficiency of 17.8%, with a V_{oc} of 0.981 V, a J_{sc} of 29.5 mA/cm^2, and a fill factor of 84.1%.

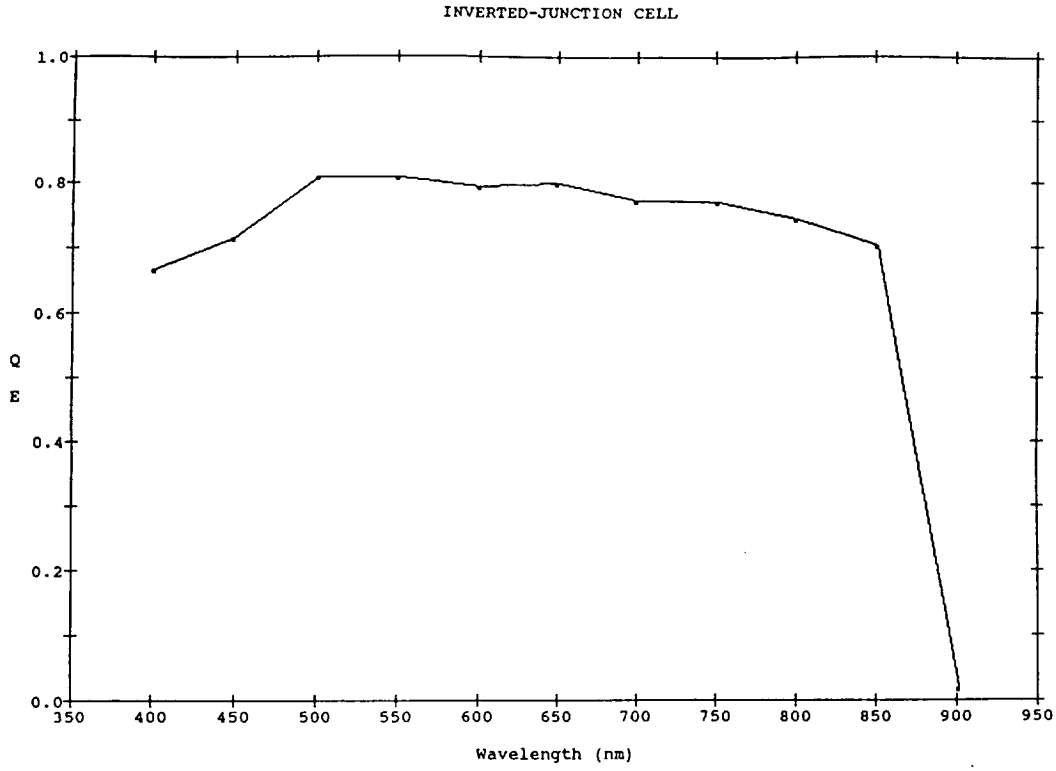

Figure 13. EXTERNAL QUANTUM EFFICIENCY OF AN INVERTED-JUNCTION CELL.

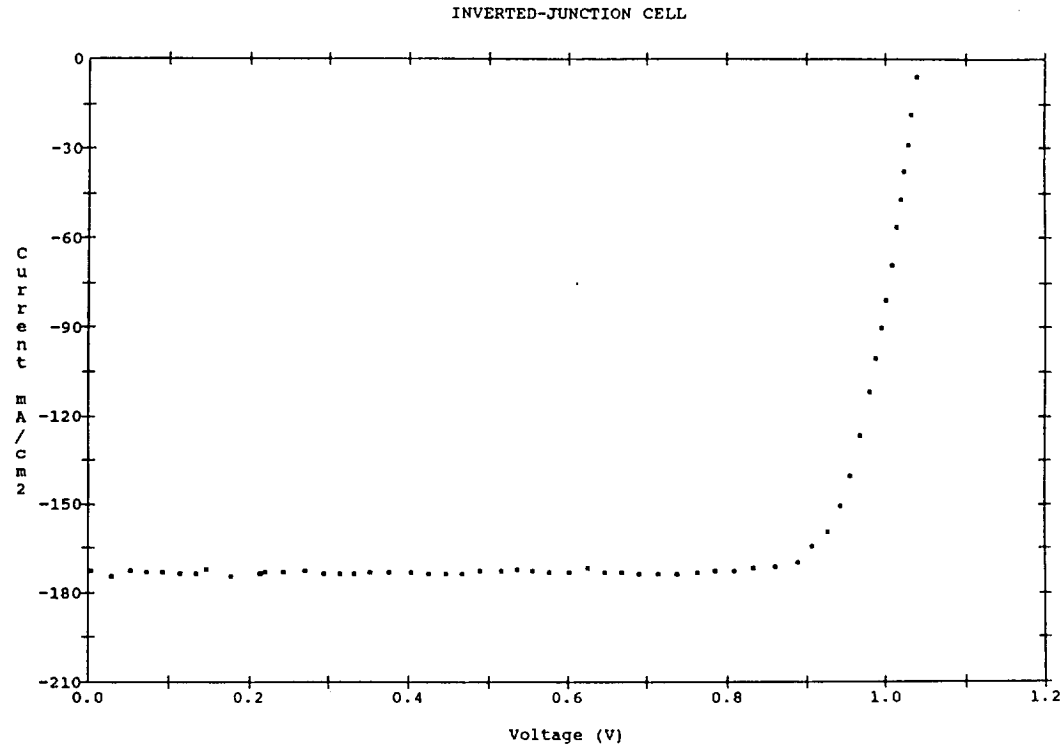

Figure 14. ILLUMINATED I-V CURVE OF THE CELL OF FIGURE 12 under about 6 suns AM0(137.2 mW/cm^2, 28°C). The cell had an efficiency of 18.8%, with a V_{oc} of 1.040 V, a J_{sc} of 172.4 mA/cm^2, and a fill factor of 84.1%.

SECTION 6: High-Efficiency CLEFT Concentrator Cell

Thin-film AlGaAs-GaAs double-heterostructure concentrator cells were fabricated which exhibit total-area conversion efficiencies as high as 23.5% AM0 at 100 suns, 25°C, measured at NASA. This solar cell structure consists of a GaAs/AlGaAs film less than 5um thick mounted to a glass cover/superstrate, with coplanar back-side contacts. The coverglass is not prismatic.

Cell Fabrication

Figure 15 is a schematic of the thin-film concentrator cell cross section. The concentrator cell structure was an AlGaAs-GaAs double-heterostructure (2) deposited on GaAs CLEFT substrates by OMCVD. The layers were deposited as follows: p+ GaAs contact layer, p+ AlGaAs back surface field, p GaAs base, n+ GaAs emitter, n+ AlGaAs window, n+ GaAs contact layer.

Frontside processing consisted of gold plating the n contact, cell area definition etch, exposure of the front window layer, and deposition of a single-layer silicon nitride AR coating. The front-contact grid was designed for 100X concentration. The front side of the wafer was then bonded to a glass superstrate and the epitaxial layers were mechanically separated from the substrate using the CLEFT process. The separation process yields an undamaged substrate that can be reused. After separation, the backside p contact was gold plated. The back metal comprised a grid that was aligned to the front grid. Etching was used to complete the definition of the cell area. The same etch step also exposed the front n metal bond pad, allowing both n and p contacts to be accessed from the backside of the cell. Finally, the glass superstrate was coated with a magnesium fluoride AR coating and the cells were diced apart.

Figure 16 shows the front and rear view of a cell. The cells have a total junction area of .126 cm^2. The n and p bus bars surround the active cell area, and are accessed from the backside. The total grid line coverage is approximately 8 percent. The total cell footprint including the contact pads is .25 cm^2. There is no optical coating on the backside of the cell, although one could be used to enhance the transmission of unabsorbed light.

The I-V measurements for the CLEFT cells were made at the NASA Lewis Research Center. One sun AM0 measurements were made using a filtered xenon solar simulator with an appropriate airplane-flown reference cell. Concentrated sunlight measurements were made using a pulsed Xenon simulator with the assumption of linearity between short-circuit current and concentration. During all measurements, the cells were mounted in a measuring block built by Kopin. The block allowed the cell, with coplanar back contact pads, to sit on four contact points (current and voltage, both plus and minus). An aperture slightly larger in diameter than the cell and anodized black was used to minimize light collection effects from the glass superstrate. During one sun measurements, the block was sitting on a temperature controlled plate held at 25°C. The light beam was shuttered off when actual data was not being taken in order to minimize any temperature rise. During concentration measurements, the pulsed simulator was on for about two milliseconds for each I-V curve, with negligible cell heating due to the light beam.

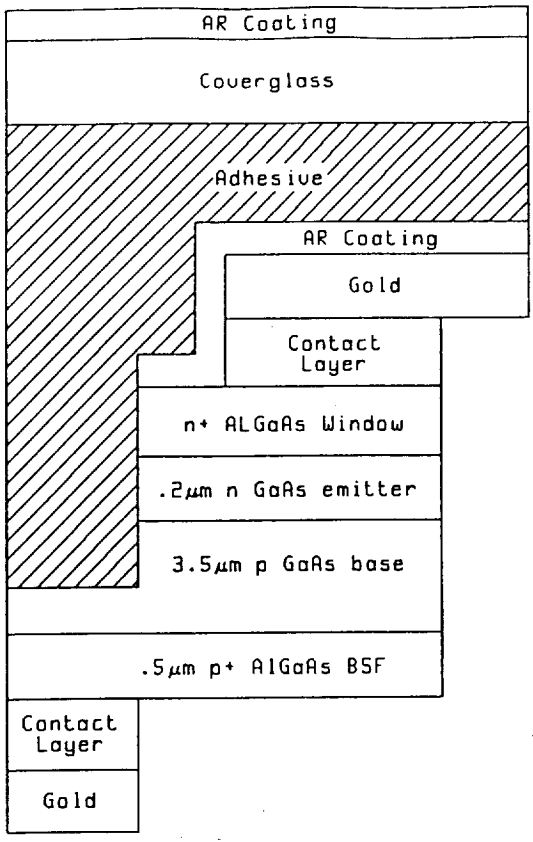

Figure 15. SCHEMATIC OF HIGH-EFFICIENCY THIN-FILM CONCENTRATOR.

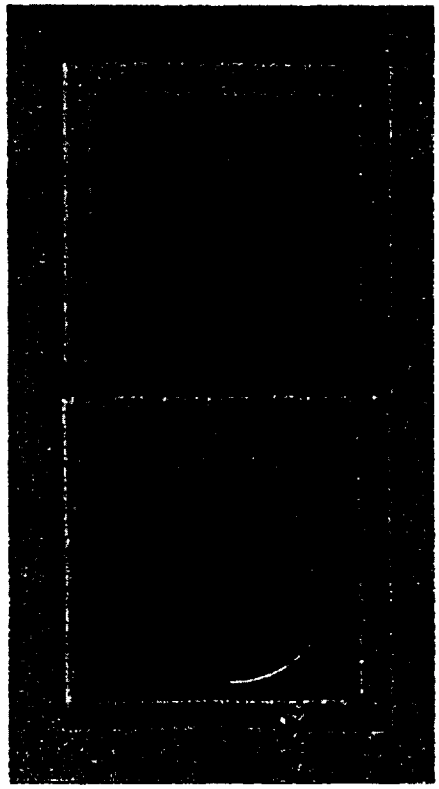

Figure 16. FRONT AND BACK VIEW OF THIN-FILM CONCENTRATOR CELL.

Cell Performance

An illuminated I-V curve of one of the best thin-film concentrator cells is shown in Figure 17. The measurement is at 100 suns, AM0, 25° C and is based on an area of .126 cm^2, corresponding to the busbar inner area. There is no junction area under either busbar. No prismatic coverglass was used. The cell shows a Voc of 1.14 volts, an Isc of 419 milliamps, and a fill factor of 84.1%, leading to a cell efficiency of 23.5%. Under one sun conditions the same cell has an efficiency of 20.5% AM0, with a V_{oc} of 0.99 volts, I_{sc} of 4.19 ma and a fill factor of 85.0% In total, 37 cells were measured with a median efficiency of 22.9% at 100X, AM0. Performance data for these cell is tabulated in Tables 7 and 8 for one-sun and concentrator illumination, respectively.

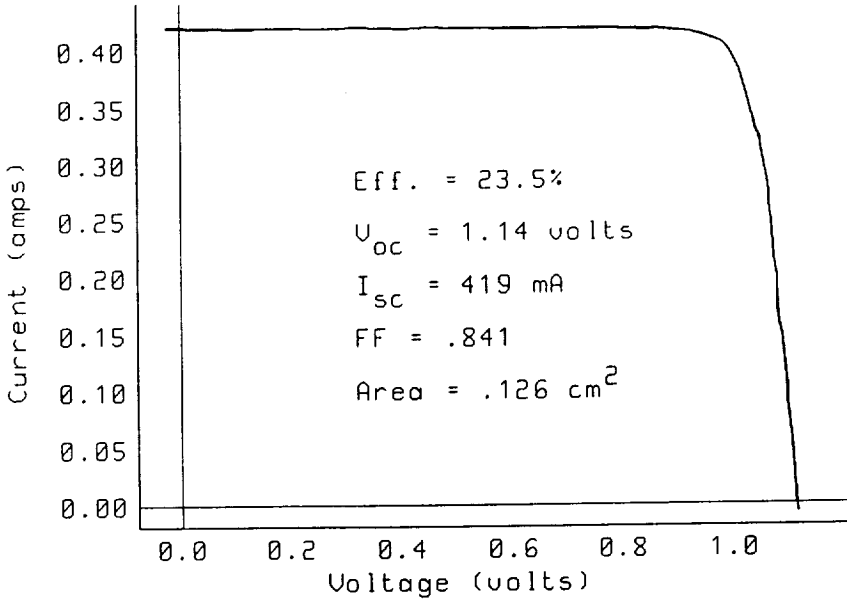

Figure 17. ILLUMINATED I-V CURVE OF A THIN FILM CONCENTRATOR AT 100X, AM0, 25C. The units of current are in amps and the bias is in volts.

Figure 18 shows a breakdown of efficiency, open circuit voltage and fill factor versus concentration for the cell in Figure 17. The cell shows an increase in efficiency up to a concentration of approximately 100X, the design concentration, at which point it begins to drop off.

The efficiency falloff is attributed to the fill factor decrease with concentration. The maximum value of fill factor is between 10X and 20X, and is limited by series resistance. Voltage is still increasing with concentration at 150X. Doubling the front and rear grid line thicknesses to reduce resistance moves the maximum fill factor to concentration of 50X. Ongoing work includes optimization of grid line thicknesses and contact layer sheet resistances in order to further improve the fill factor response with concentration.

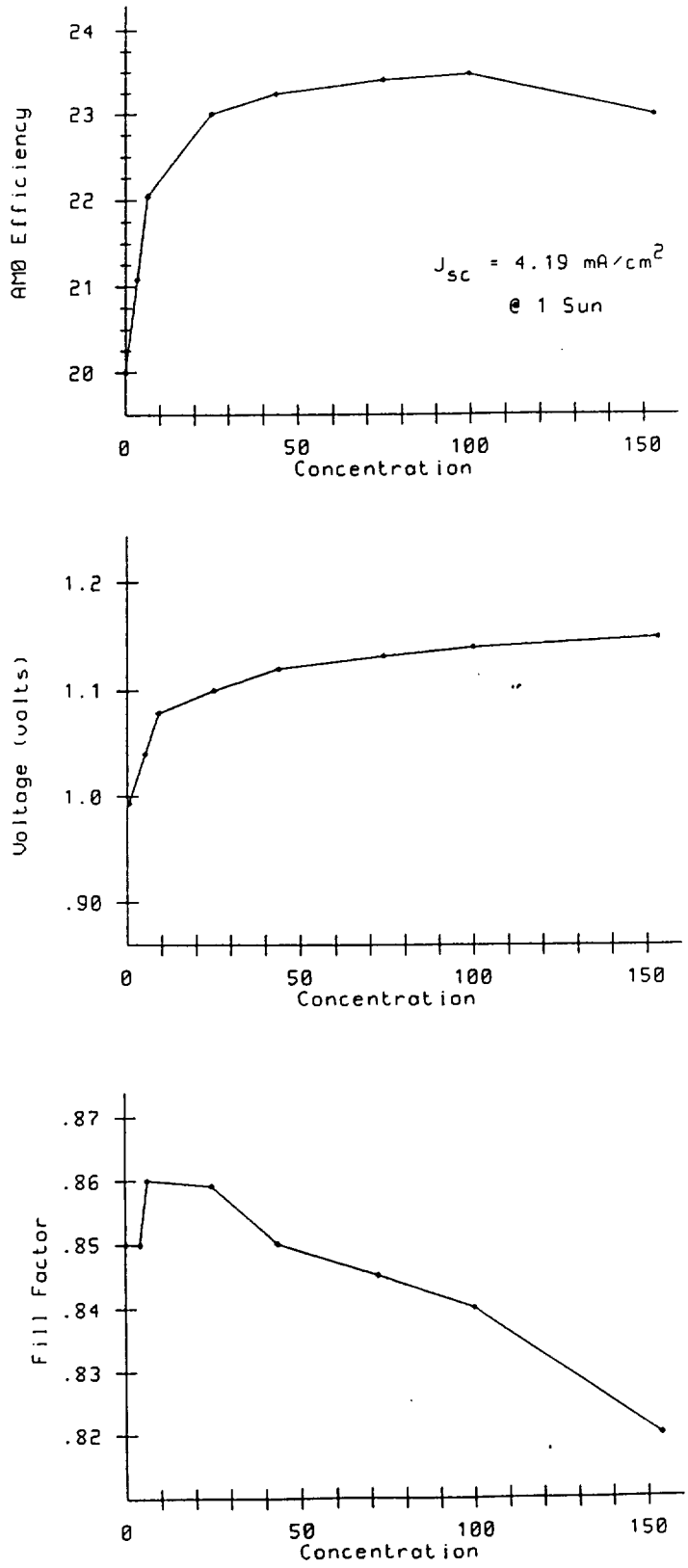

Figure 18. EFFICIENCY, V_{OC}, AND FILL FACTOR FOR THE THIN-FILM CONCENTRATOR cell in figure 17 as a function of concentration.

TABLE 7

ONE-SUN I-V DATA FOR THIN-FILM CONCENTRATORS

Cell ID		Isc mA	Voc V	Pmax mW	Fill	Eff %
2	D	4.20	0.993	3.56	0.855	20.73
2	E	4.20	0.989	3.55	0.855	20.64
2	G	4.21	0.985	3.53	0.850	20.51
3	C	4.18	0.982	3.45	0.841	20.07
3	D	4.18	0.992	3.53	0.851	20.53
3	E	4.22	0.988	3.54	0.849	20.59
3	H	4.12	0.986	3.46	0.852	20.12
4	D	4.21	0.992	3.54	0.846	20.56
4	E	4.19	0.990	3.52	0.849	20.47
4	G	4.19	0.988	3.52	0.849	20.45
4	I	4.05	0.983	3.25	0.817	18.91
4	J	4.19	0.962	3.20	0.793	18.60
5	A	4.17	0.989	3.48	0.845	20.25
5	B	4.19	0.992	3.53	0.850	20.53
5	E	4.16	0.988	3.35	0.814	19.46
5	G	4.21	0.991	3.55	0.852	20.66
6	A	4.14	0.987	3.46	0.848	20.14
6	B	4.21	0.992	3.56	0.851	20.68
6	G	4.18	0.988	3.52	0.851	20.45
7	A	4.13	0.986	3.46	0.850	20.12
7	B	4.19	0.991	3.55	0.854	20.63
7	F	4.17	0.988	3.52	0.854	20.47
7	G	4.13	0.985	3.47	0.854	20.20
7	H	4.02	0.980	3.35	0.851	19.49
8	C	4.21	0.988	3.50	0.842	20.36
8	E	4.19	0.993	3.56	0.855	20.67
8	F	4.20	0.985	3.51	0.847	20.39
8	G	4.13	0.952	3.48	0.855	20.24
9	B	4.18	0.981	3.50	0.852	20.32
9	E	4.18	0.989	3.54	0.855	20.56
10	C	4.14	0.986	3.46	0.848	20.12
10	D	4.16	0.987	3.48	0.848	20.24
10	E	4.17	0.986	3.51	0.853	20.41
10	F	4.13	0.985	3.47	0.853	20.18
10	G	4.09	0.984	3.45	0.857	20.06
11	F	4.06	0.982	3.39	0.849	19.69
11	G	4.01	0.983	3.35	0.850	19.48

Note: Measurements were made at NASA Lewis Research Center courtesty of D. Brinker and H. Curtis.

TABLE 8

100X CONCENTRATOR PERFORMANCE FOR THIN-FILM CELLS

Cell ID	Conc.	Isc mA	Voc V	Pmax mW	Fill	Eff %	n value
2 D	100.2	420.75	1.142	400.88	0.835	23.27	1.26
2 E	99.4	417.35	1.139	394.83	0.831	23.11	1.27
2 G	99.7	419.71	1.139	395.99	0.828	23.10	1.34
3 C	100.7	420.88	1.140	401.66	0.837	23.20	1.34
3 D	100.1	418.40	1.141	396.18	0.830	23.02	1.26
3 E	99.5	419.93	1.141	394.67	0.824	20.12	1.29
4 D	99.3	417.92	1.140	393.00	0.825	23.02	1.25
4 E	99.9	418.62	1.140	391.39	0.820	22.78	1.27
4 G	100.2	419.90	1.140	392.34	0.819	22.77	1.29
4 I	99.9	404.40	1.135	385.68	0.840	22.46	1.29
4 J	100.6	421.48	1.134	393.55	0.824	22.75	1.45
5 A	99.8	416.28	1.139	399.23	0.842	23.26	1.27
5 B	100.3	420.25	1.142	402.19	0.838	23.32	1.27
5 E	99.8	414.44	1.137	386.59	0.817	22.51	1.28
5 G	99.9	420.51	1.142	394.43	0.821	22.96	1.28
6 A	100.2	414.97	1.137	397.38	0.842	23.06	1.27
6 B	99.7	419.91	1.142	401.61	0.838	23.42	1.27
6 G	100.5	420.10	1.141	391.53	0.817	22.66	1.29
7 A	100	413.03	1.138	396.36	0.844	23.05	1.28
7 B	100	418.84	1.141	400.98	0.839	23.33	1.27
7 F	99.9	416.65	1.141	390.87	0.822	22.75	1.29
7 G	100.4	414.77	1.139	390.57	0.827	22.62	1.3
7 H	99.6	400.23	1.138	381.51	0.838	22.28	1.33
8 C	100.7	423.80	1.142	403.82	0.834	23.33	1.3
8 E	100.6	421.57	1.143	397.77	0.826	22.99	1.27
8 F	99.4	417.46	1.139	392.31	0.825	22.95	1.3
8 G	100.2	413.81	1.138	389.53	0.827	22.61	1.29
9 B	100.5	420.27	1.141	402.51	0.840	23.28	1.34
9 E	99.6	416.40	1.141	394.00	0.830	23.00	1.28
10 C	100.2	414.76	1.138	396.12	0.839	22.99	1.29
10 D	100.3	417.35	1.138	398.87	0.840	23.12	1.28
10 E	99.7	415.86	1.139	396.00	0.836	23.09	1.3
10 F	100.2	413.87	1.139	394.88	0.838	22.92	1.3
10 G	100.3	410.16	1.138	392.04	0.840	22.73	1.3
11 F	100.3	407.22	1.139	390.77	0.842	22.66	1.33
11 G	100.2	401.84	1.139	385.29	0.842	22.36	1.32

Note: Measurements were made at NASA Lewis Research Center courtesty of D. Brinker and H. Curtis.

SECTION 7: Conclusion

We have achieved the goal to demonstrate a high-efficiency thin-film space concentrator cell. We have used the CLEFT process to fabricate AlGaAs-GaAs double heterostructure concentrator cells which are less than 5 um thick and mounted to a coverglass. These cells are of interest due to their superior performance and thermal-control advantages. The best cell had a total area conversion efficiency of 23.5% AMO, at 100X, 25°C as measured by NASA.

The specific objectives of this contract were the development of materials and device technology necessary to make possible such a cell. The technology developed here includes:

- Improved quality, high-diffusion length, thin-film GaAs,
- Investigation of patterned junction formation,
- Development of a high-efficiency, inverted-junction cell with a junction depth of over 3 um,
- Development of co-planar p- and n-contact high-efficiency thin-film GaAs concentrator cells.

The objectives of the tasks have been achieved, and the project has resulted in the fabrication of high-efficiency thin-film concentrator cells.

REFERENCES

1. R.W. McClelland, C.O. Bozler, and J.C.C. Fan, Applied Physics Letter 37 (1980) P. 560.

2. C.O. Bozler, R.W. McClelland, and J.C.C. Fan, IEEE Electron Devices Letter EDL-2 (1981) P. 203.

3. J.C.C. Fan, R.W. McClelland, and B.D, King, Proc. 17th IEEE Photovoltaic Specialists Conf., Kissimmee, FL 1984, (IEEE, New York, 1984) P. 31.

4. R.K. Ahrankiel, D.J. Dunlavy, J. Benner, R.P. Gale, R.W. McClelland, J.V. Gormley, B.D. King, Applied Physics Letters 53 (1988) P. 598.

APPENDIX

Copies of the following papers are included for reference:

"Concepts for Thin-film GaAs Concentrator Cells," M.B. Spitzer, R.P. Gale, R.W. McClelland, B.D. King, J. Dingle, and R. Morrison, Rec. of the 24th Intersociety Energy Conversion Engineering Conference, 1989.

"23.5% Efficient Space Concentrator Cells," B. D. Dingle, R. P. Gale, R W. McClelland, and M. B. Spitzer, Rec. of the 21st IEEE Photovoltaic Specialists Conference, 1990.

Concepts for Thin-Film GaAs Concentrator Cells

M. B. Spitzer
R. P. Gale
R. McClelland
B. King
J. Dingle
R. Morrison

Reprinted from
PROCEEDINGS OF THE 24TH INTERSOCIETY ENERGY CONVERSION ENGINEERING CONFERENCE
Vol. 2, No. 1, August 1989

CONCEPTS FOR THIN-FILM GaAs CONCENTRATOR CELLS

M. B. Spitzer, R. P. Gale, R. McClelland,
B. King, J. Dingle, and R. Morrison

Kopin Corporation
Taunton, Massachusetts 02780

ABSTRACT

This paper reports on the development of advanced GaAs concentrator solar cells, and in particular, on the use of CLEFT processes for formation of thin-film structures. The use of CLEFT has made possible processing of the back, and cells with back surface grids are discussed. Data on patterned junction development are presented; such junctions are expected to be useful in back surface applications requiring point-contacts, grating structures, and interdigitated back contacts. We report here for the first time CLEFT concentrator solar cells with grids on the front and back surfaces; these cells are 4μm thick and are bonded to glass covers for support. Air mass zero efficiency of 18.8% has been obtained for a CLEFT concentrator operating at 18.5 suns.

1. INTRODUCTION

Future photovoltaic space power systems require advanced cells of the highest possible efficiency. In addition, such photovoltaic power systems must endure space radiation environments with predictable and small degradation. For these reasons, research on advanced light-weight cells is of considerable current interest. Cells made from gallium arsenide (GaAs) are well-suited to these requirements.

One approach to both high radiation-resistance and improved efficiency comprises use of concentrating optics which, with proper design, can offer increased radiation shielding. In addition, operation under concentration yields higher conversion efficiency, provided that series resistance losses remain low. Of course, in such an approach, the weight of the power system becomes a function of the cell *and* its optics, rather than the cell itself.

A further desirable attribute of advanced solar cells is low cell cost. For the case of GaAs, a significant cost driver is the price of the substrates. One approach to reducing this cost comprises the removal and reuse of the substrate via the Cleavage of Lateral Epitaxial Films for Transfer (CLEFT) technique[1], and use of this approach will be descibed below. CLEFT yields the recovery and reuse of the substrate, but there is a further important reason for using CLEFT for space solar cells: the CLEFT technique (as well as other substrate removal techniques) makes possible the processing of the electrically and optically active back side of the *p/n junction or solar cell base*, whereas in conventional GaAs cells, one is limited to processing the back of the *substrate*. Thus, substrate
removal techniques permit utilization of advanced designs such as:

- active back surface reflectors,
- back contact pad access for p and n contacts,
- coplanar interdigitated back contacts, and
- reduced junction area.

In this paper, we will describe research to improve cell efficiency by using the above approaches in a concentrator design. We will show that the CLEFT approach can be used successfully for fabrication of high efficiency light weight space cells, and we will report on concentrator cells with back surface grids.

2. BACKGROUND

To make clear some of the concepts and results to be reported on in later sections, we first provide a brief review of the CLEFT technique[1-3]. The CLEFT process permits the growth of thin single-crystal GaAs films by chemical vapor deposition on reusable GaAs substrates. Since many films can be obtained from one substrate, this process permits a reduction in material usage and cost. Since single-crystal films are used, cell efficiencies remain high, as we will show below. The films are only a few microns thick; therefore such cells can have very high power-to-weight ratios. Films with thickness of less than 1 μm have been produced, and thick films of up to 20μm have been made as well. Thus, use of the CLEFT process does not introduce constraints on the solar cell thickness, which owing to this versatility, may be optimized.

The CLEFT process is one of several peeled-film techniques. The basic steps in peeled-film technology are: The growth of a thin single-crystal epilayer on a single-crystal substrate, the separation of the epilayer from the substrate, and if low cost is the objective, the reuse of the

CH2781-3/89/0000-0785 $1.00 © 1989 IEEE

recombination velocity is much lower than v_D, suggesting that thinning will reduce the overall recombination in the cell. Use of more lightly doped GaAs is expected to yield somewhat higher diffusion length. Analysis of CLEFT material is in progress.

3.2 Junction Patterning Considerations

One important factor concerning the fabrication of grating or point-contact cells with restricted junction area is the development of techniques for forming the junctions. Planar approaches that are consistent with fine-line photolithography would be especially useful. One technique that would be useful is ion implantation of Be and Zn for p^+ regions, and Si for n^+ regions; however, little work has been published on the application of these implants to GaAs solar cells. The primary difficulty in the development of ion implantation is the optimization of the anneal process, which must activate the dopant and repair the crystal damage caused by the ion implantation.

To simplify the development of anneal processes, we have ion-implanted wafers that were then fabricated into solar cells that are stable during high temperature cycling[10]; this type of cell structure allowed us to to anneal the implant damage after cell fabrication and dicing. In this way, we were able to examine a range of anneal parameters without fabricating an inordinately large number of wafers. The solar cell endurance during high temperature cycling has been described elsewhere[10]; here we note only that the contact and encapsulation system makes possible the cycling of the structure to temperatures exceeding 700°C for up to 30 min. We note that in the cell structures used here, no attempt was made to optimize the AR coating (which was used for encapsulation) or the junction depth. SIMS analysis indicates that the junction is too deep for high current collection efficiency and that performance could be improved by using anodic oxidation and stripping to thin the junction. We have not pursued this because we are interested in back junctions, for which current collection is far less important.

Table 2 indicates the solar cell performance results obtained thus far from ion-implanted homojunctions formed as described above. Note that we are primarily concerned with V_{OC} and FF. The FF are fairly good indicating low parasitic resistance losses. The V_{OC} data are lower than one would like for high performance cells; we speculate that this is a result of inadequate encapsulation during the anneal, leading to As depletion in the near-surface region, and this factor is being examined further. It should be noted that the encapsulation coating was not fully optimized for AR performance, and that a cell from which the coating was removed yielded only a 10% reduction on J_{SC}. Although the investigation of patterned junctions is not complete, it appears at present that this work can lead to a simple means to pattern the junctions.

4. CLEFT CONCENTRATOR FABRICATION AND TESTING

Results to date on actual CLEFT solar cells have been quite good. Elsewhere, we have reported on $2x2cm^2$ CLEFT cells with one-sun AM0 efficiency exceeding 19%[3]. Concentrator cells have also been formed in CLEFT material, and we report here for the first time the performance results for these cells.

The concentrator cells are formed in the following way: First the active layers were grown on a wafer that was properly patterned for CLEFT. Second, the front grids and busbars were formed; the circular busbar defined the border of the active GaAs volume. AR coating was next deposited. The wafer was then bonded to a glass cover and mechanically separated from the substrate. The glass cover provided mechanical support after the separation step. Back grids and busbars were then applied using photolithography to form fine-line patterns that were closely aligned to the front grids. Cells with full area back metallization were also formed.

After the formation of the back metallization, excess inactive GaAs was removed from regions beyond the busbars. This permitted contact to be made to the front metallization from the back side, as shown in Figure 2. The cells are circular and have an light-receiving area of $0.126cm^2$. The shadow loss is about 8%. The cover glass was not AR-coated and was characterized by reflection loss of approximately 6%.

The cells were tested under simulated AM0 insolation ($137.2\ mW/cm^2$). Since these cells are covered by glass that is larger than the light-receiving area, care was taken to mask the incident light soas to expose *only* the primary light-receiving area. It was found that if the glass is fully exposed to the light, the incident intensity would be artificially high, owing to light collection by the glass via total internal reflection. Also, unless the light is masked, a significant amount of scattered light can enter the rear surface and increase the current.

Figure 3 shows the I-V characteristic of a CLEFT concentrator under 18.5 suns AM0 illumination. This cell has an ordinary grid on the front, and a full-area Au metal contact on the back. The efficiency is 17.8% at one sun and 18.8% at 18.5 suns. Figure 4 shows the results of a first attempt to fabricate a transparent CLEFT concentrator cell with grids on both sides. Although the J_{SC} is limited, perhaps because the cell is too thin, the fabrication experiment shows that the CLEFT process is suitable for two-sided processing of the type needed for the advanced structures. Although extensive analysis of the performance of these cells has yet to be made, the efficiencies thus far obtained are a strong indicator of the potential of this approach.

TABLE 2

BEST ONE-SUN and DARK CURRENT RESULTS
FOR ION-IMPLANTED JUNCTIONS

ION SPECIES	TYPE	ANNEAL TEMP(°C)	ANNEAL TIME(min)	J_o(1) (mA/cm^2)	Voc (mV)	Jsc(2) (mA/cm^2)	FF (%)
Be	p^+	700	1	$1.0x10^{-13}$	856	18.2	79.4
Zn	p^+	750	15	$5.1x10^{-14}$	880	24.4	78.2
Si	n^+	800	10	$1.6x10^{-14}$	900	19.1	80.1

Notes: (1)J_o estimated from V_{oc}-J_{sc} data. (2) Insolation was AM0, $137mW/cm^2$

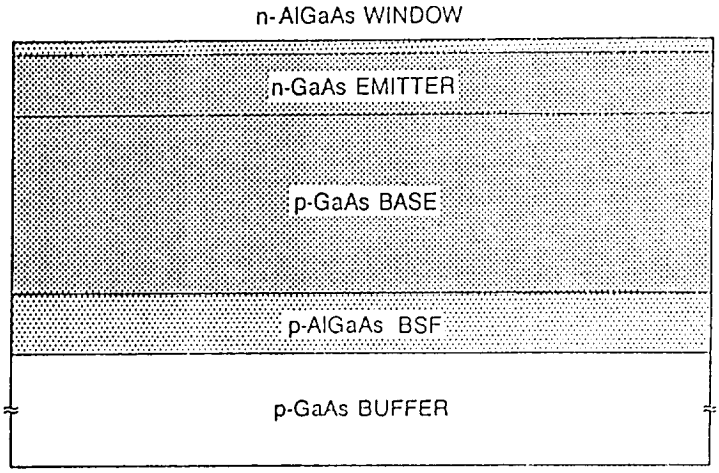

Figure 1. DOUBLE HETEROSTRUCTURE CELL DESIGN. The AlGaAs is used to reduce the recombination velocity at the boundaries of the absorbing GaAs region.

23.5% THIN-FILM SPACE CONCENTRATOR CELLS

B. D. Dingle, R. P. Gale, R. W. McClelland, and M. B. Spitzer

Kopin Corporation

and

H. B. Curtis and D. J. Brinker

NASA Lewis Research Center

Presented at the 21st IEEE Photovoltaic Specialists Conference
May 1990, Orlando, Florida

Kopin Corporation
695 Myles Standish Boulevard
Taunton, Massachusetts 02780

23.5% THIN-FILM SPACE CONCENTRATOR CELLS

B. D. Dingle, R. P. Gale, R. W. McClelland, and M. B. Spitzer
Kopin Corporation, Taunton, MA 02780

H. B. Curtis and D. J. Brinker
NASA Lewis Research Center, Cleveland, OH 44135

ABSTRACT

GaAs is a strong contender for use in space photovoltaic power systems due to its high conversion efficiencies, radiation hardness, and developed processing technology. Thin-film AlGaAs-GaAs double-heterostructure concentrator cells were fabricated which exhibit total-area conversion efficiencies as high as 23.5% AM0 at 100 suns, 25°C, measured at NASA. This is one of the best space concentrators measured to date at NASA and is for a thin-film cell without a prismatic coverglass. This solar cell structure consists of a GaAs/AlGaAs film less than 5um thick mounted to a glass cover/superstrate, with coplanar back-side contacts. The coverglass is not prismatic. We use the CLEFT process, a method for mechanically separating epitaxial layers from their substrate, to process these cells into thin-films. We thereby retain the advantages of single-crystal GaAs while reducing weight and cutting cost by allowing for substrate reuse. Thin film cells also have better thermal management capabilities and can be stacked for use in tandem structures. Cell fabrication and performance are described, and directions for further improvements are identified.

INTRODUCTION

We have routinely used the CLEFT (1) process to produce thin film semiconductor materials up to three inches in diameter and less than 10 μm thick. CLEFT is an established process which entails the mechanical separation of the epitaxial film from its substrate. This approach has the benefit of allowing for substrate reuse, thereby reducing the overall cell material cost. We have now applied the CLEFT process to the fabrication of concentrator cells in order to take advantage of the inherent benefits of thin-film cells. By "thin-film" we mean layers less than 10 μm thick that are removed entirely from a single crystal substrate. Thin-film concentrator cells are of interest because they require less than 5 μm of semiconducting material and their efficiencies are now comparable to cells on bulk substrates.

The extremely thin nature of these cells also allows for low weight and superior thermal management. Heat sinking can be more efficient because it can be placed in closer proximity to the junction. Since the cells are transparent to long wavelenths, infra-red radiation which enters the cell can be transmitted directly to a back-side heat sink or, alternatively, reflected out the front of the cell by using a back surface reflector. A back surface reflector could also be tailored to reflect photons with energy above the band edge, thus providing a double-pass for more weakly absorbed light, thereby doubling the effective material thickness. Ultimately, thin film cells can be expected to yield higher efficiencies than conventional cells owing to light trapping possibilities and lower operating temperature. These thin film cells also lend themselves well to tandem structures and advanced structures involving reflectors and coplanar contacts.

EXPERIMENTAL

Figure 1 is a schematic of the thin-film concentrator cell cross section. The concentrator cell structure was an AlGaAs-GaAs double-heterostructure (2) deposited on GaAs CLEFT substrates by OMCVD. The layers were deposited as follows: p+ GaAs contact layer, p+ AlGaAs back surface field, p GaAs base, n+ GaAs emitter, n+ AlGaAs window, n+ GaAs contact layer.

Frontside processing consisted of gold plating the n contact, cell area definition etch, exposure of the front window layer, and deposition of a single-layer silicon nitride AR coating. The front-contact grid was designed for 100X concentration. The front side of the wafer was then bonded to a glass superstrate and the epitaxial layers were mechanically separated from the substrate using the CLEFT process. The separation process yields an undamaged substrate that can be reused. After separation, the backside p contact was gold plated. The back metal comprised a grid that was aligned to the front grid. Etching was used to complete the definition of the cell area. The same etch step also exposed the front n metal bond pad, allowing both n and p contacts to be accessed from the backside of the cell. Finally, the glass superstrate was coated with a magnesium flouride AR coating and the cells were diced apart.

RESULTS AND DISCUSSION

An illuminated I-V curve of one of the best thin-film concentrator cells is shown in Figure 3. The measurement is at 100 suns, AM0, 25° C and is based on an area of .126 cm^2, corresponding to the busbar inner area. There is no junction area under either busbar. No prismatic coverglass was used. The cell shows a Voc of 1.14 volts, an Isc of 419 milliamps, and a fill factor of 84.1%, leading to a cell efficiency of 23.5%. This is one of the best space concentrator cell efficiencies that NASA has measured as yet for cells without a prismatic coverglass at AM0, 100 suns. In total, 40 cells were measured with a median efficiency of 22.9% at 100X, AM0. Under one sun conditions the same cell has an efficiency of 20.5% AM0, with a V_{oc} of 0.99 volts, I_{sc} of 4.19 ma and a fill factor of 85.0%

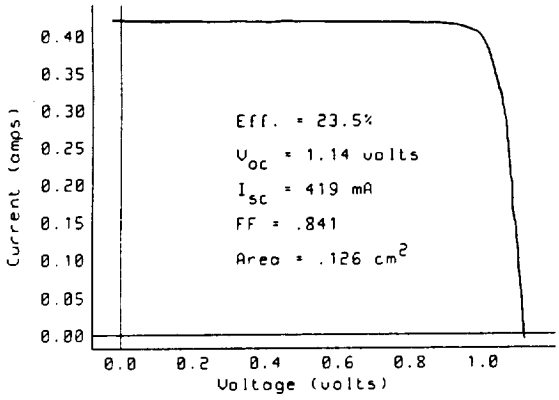

Figure 3: Illuminated I-V curve of a thin film concentrator at 100X, AM0, 25C. The units of current are in amps and the bias is in volts.

Figure 4 shows a breakdown of efficiency, open circuit voltage and fill factor versus concentration for the cell in Figure 3. The cell shows an increase in efficiency up to a concentration of approximately 100X, the design concentration, at which point it begins to drop off.

The efficiency falloff is attributed to the fill factor decrease with concentration. The maximum value of fill factor is between 10X and 20X, and is limited by series resistance. Voltage is still increasing with concentration at 150X. Doubling the front and rear grid line thicknesses to reduce resistance moves the maximum fill factor to concentration of 50X. Ongoing work includes optimization of grid line thicknesses and contact layer sheet resistances in order to furthur improve the fill factor response with concentration.

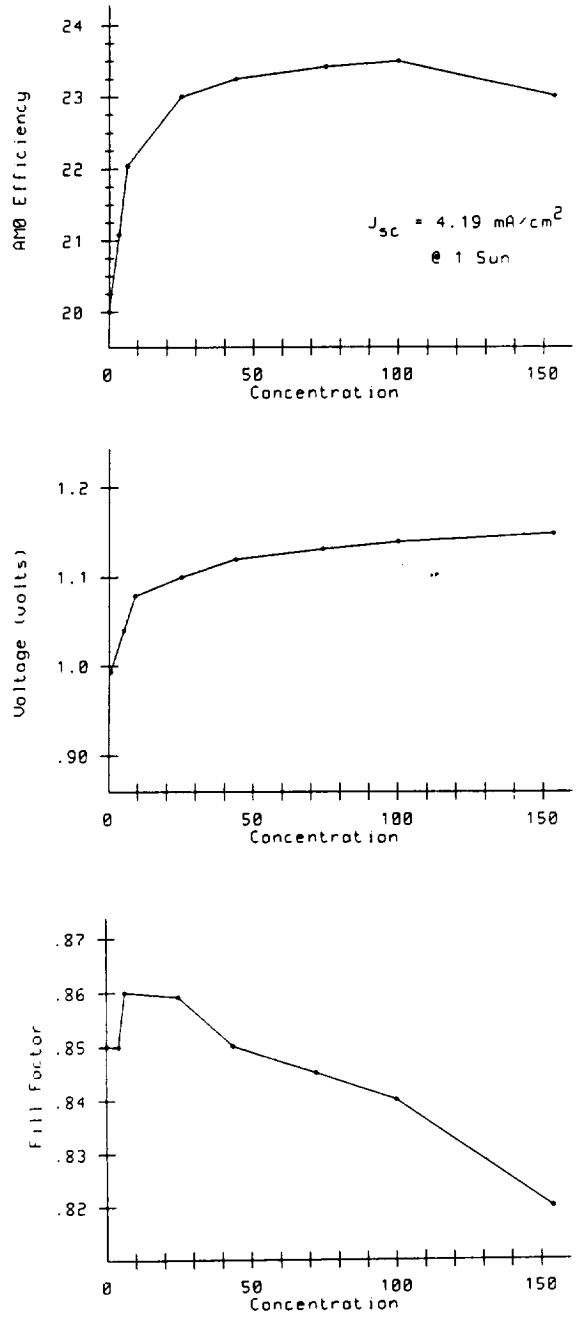

Figure 4: Efficiency, V_{oc}, and fill factor for the thin-film concentrator cell in figure 3 as a function of concentration.